Stereological Analysis of Micromechanical Behavior of Concrete

Kamran M. Nemati

Associate Professor, Departments of Construction Management / Civil Engineering, University of Washington, Seattle, Washington 98195, U.S.A.

Piet Stroeven

Professor, Faculty of Civil Engineering, Delft University of Technology; The Netherlands.

ABSTRACT:
To study micromechanical behavior of concrete, stereological measurements were conducted, i.e., crack orientation, length, density and other features. A special experimental technique was developed which made possible the preservation of the compressive stress-induced microcracks in concrete as they exist under applied loads. This technique involved injecting a molten-metal alloy into the induced cracks and solidifying it before unloading. Scanning Electron Microscopy (SEM) was employed to capture images from the cross sections of the concrete specimens.

INTRODUCTION

The Scanning Electron Microscope (SEM) is one of the most versatile instruments available for the examination and analysis of microstructural characteristics of solid objects. The primary reason for the SEM's usefulness is the high resolution that can be obtained when bulk objects are examined.

The microscope has been a powerful tool in the study of cement and concrete since the early development of these materials [1, 2]. The electron microscope was apparently first used to study the hydration process of concrete [3, 4, 5, 6]. Although most of these studies were not directly related to cracks, they led the way to later studies of cracks in which electron microscopy was a powerful tool. Later on the scanning electron microscope was used to observe the growth of surface cracks during loading, using magnifications generally from 35× to 450× [7]. This investigation of microcracking ranges from a macroscopic studies of the behavior of cracked specimens to a microscopic study of the cracks themselves. The presence of microcracks was predicted on the basis of macrobehavior and verified by microscopic study. In this paper, the application of stereology to the microstructure of concrete will be examined.

TECHNIQUE TO PRESERVE STRESS-INDUCED CRACKS IN CONCRETE

The experimental technique utilized for this research involves the application of a metal in liquid phase, Wood's metal, which has a melting point range from 70°C to 88°C to preserve the microstructure of stress-induced microcracks in concrete. Wood's metal has a Young's modulus of 9.7 GPa, a density of 9.4 g/cm^3, and an effective surface tension of about 400 mN/m, and is solid at room temperature. Used in conjunction with scanning electron microscopy, it has made possible the detailed observation of microcracks in concrete as they exist under load. Details of the experimental technique is reported in detail elsewhere [8, 9, 10, 11]. Three normal-strength concrete cylinders, 203 mm long by 102 mm in diameter, were cast using the mix designs shown below.

Cement: 346 Kg/m^3
Water: 183 Kg/m^3
Coarse Aggregate (Pea Gravel): 979 Kg/m^3
Sand: 859 Kg/m^3
Admixture: HRWR
W/C: 0.528
Slump: 38 mm
Ultimate Strength: 51.7 MPa

The concrete cylinder ends were ground parallel to one another. The confining stress used to generate triaxial compression was supplied by stainless steel wires, 0.3 mm in diameter, that were wound around the entire length of the concrete cylinders, at a pre-tension of 670 N. Three experiments were conducted: one on a sample subjected to no loads and two different loading conditions, uniaxial and triaxial, were used to induce cracks in the other two concrete cylinders. Triaxiality was provided by the wire wound around the concrete cylinder. Specimens were loaded to 85 to 90% of the ultimate strength.

After the concrete samples were prepared for scanning electron microscope studies, backscatter electron (BSE) images were extracted from each sample. Figure 1 shows a typical BSE micrograph which is a multiphase image consisting of bulk cement paste, aggregates, and Wood's metal representing stress-induced microcracks. In order to recognize and isolate Wood's metal, which is the representative of pores and fractures in concrete, using an image analyzer, a histogram for all of the different phases in the image based on their gray levels can be produced,

with zero representing the darkest phase and 255 representing the brightest phase (Figure 2). From this histogram, and by means of the trial and error method, two threshold levels can be established to encompass the brightest phase in the image, namely Wood's metal. The threshold for Wood's metal identification was set between 170 and 255. The next step is to eliminate objects from the background that don't fall between these threshold levels. Once the above task is accomplished, what is left in the image is the crack network and pores indicated by Wood's metal. At this point the aim is to eliminate objects on the basis of their area in pixel units. The lower and upper limits of the objects to be eliminated has to be established to include small pores, small non-continuous cracks, etc. The next step is to transform this image into a skeletonized binary image by means of a binary thinning process. For every thinning step, pixels that are not relevant to the connectivity of an object are removed from the object margins, i.e., converted into background pixels. The connectivity of objects is thus maintained. This process can be continued until all objects are reduced to a width of one pixel that approximates the skeletons. Figure 3 is the final binary image used for stereological measurements.
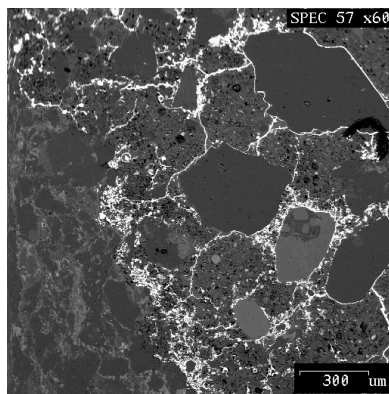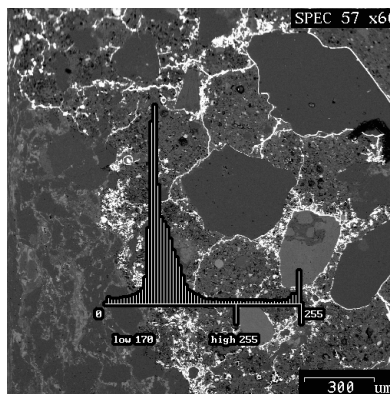

Figure 1 A SEM backscatter image

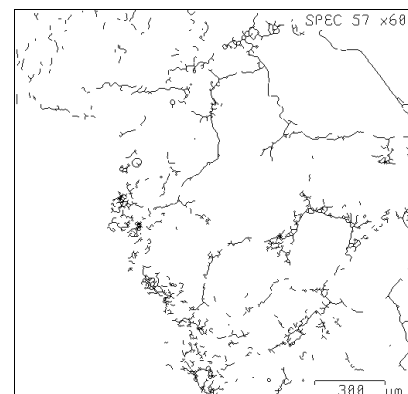**Figure 2** Establishing threshold in histogram

Figure 3 Binary-thinned image of the crack network in concrete

STEREOLOGY AND CONCRETE

All matter can be described in terms of zero, one, two, and three dimensions. Stereology deals with the interpretation of three-dimensional structures by means of their two-dimensional sections. Stereology is the opposite of photogrammetry, which utilizes three-dimensional images in order to construct flat maps. Techniques conventionally used for studying the three-dimensional structure of materials, particularly in other material sciences, are often stereological ones [12, 13].

If a sectioning plane cuts a three-dimensional aggregate of space-filling polyhedrons, a two-dimensional structure that consists of area-filling polygons can be observed. The task then is to relate the observations made on a section to the true three-dimensional microstructure. Stereology attempts to characterize numerically the geometrical and statistical aspects of those features of the microstructure of interest; for example, the microcracks in concrete. In its broadest context, stereology includes not only the quantitative study and characterization of any spatial structure, but also its qualitative interpretation.

There are various approaches to stereological problems. The statistico-geometrical approach depends on measuring and classifying a large number of two-dimensional images and is the method utilized in this study. It is applicable when objects are randomly distributed in space. In such cases, a single section, if extensive enough to contain a statistically significant number of features, may suffice to obtain valid results. It can also be used/applied in case of non-randomly distributed phases. In that case the sampling procedure should be randomized, however.

In this study, we deal with the numerical or quantitative characterization of points, lines, surfaces, and volumes. Fundamental expressions have been determined which relate measurements on two-dimensional sections to the three-dimensional structure.

BASIC MEASUREMENTS

Table 1 presents some of the basic symbols commonly used in the measurements employing quantitative stereology.

Table 1 List of basic stereological symbols and their definition

Symbol	Dimensions	Definition
P		Number of point elements, or test points
P_L	μm^{-1}	Number of intersections of cracks in a section with a superimposed test array of equally spaced straight parallel lines per unit of line length
$P_L(q)$	μm^{-1}	Number of intersection of cracks in a section with a system of equally spaced test array of straight parallel lines positioned in such a way that it successively encloses an angle θ, $\theta=\pi/2$ and $\theta=0$, respectively, with the axis of symmetry
L	μm	Length of lineal elements, or test line length
L_A	$\mu m/\mu m^2$	Total crack length in a section per unit of area
A	μm^2	Planar area of intercepted features, or test area
S	μm^2	Surface or interface area (not necessarily planar)
S_V	$\mu m^2/\mu m^3$	Total crack surface area per unit of volume $\left(\dfrac{S}{V_T}\right)$
N_A	μm^{-2}	Number of cracks in a section per unit of area
V_T	μm^3	Volume of three-dimensional features, or test volume

In this paper, the stereological parameters of P_L, L_A, and S_V will be used to perform the stereological analysis. Underwood [12] derived the relationships between L_A and S_V with P_L, which is presented below:

- **Number of Point Intersections,** P_L, is the number of points (intersections) generated per unit length of test lines, if a linear test array is applied randomly to the microstructure in the section plane.

- **Surface-to-Volume Ratio,** S_V, is the surface-to-volume ratio of a system of surfaces in a volume. The basic equation for obtaining the area of surfaces in a volume was derived by Salitikov [14] and later by Smith and Guttman [15] which is:

$$S_V = 2P_L \quad mm^2 / mm^3 \qquad (1)$$

Equation 1 applies to a system of surfaces with any configuration. It is as valid for systems of interconnected surfaces as for systems of discontinuous, separated, or bounded surfaces. Equation 1 was derived by considering a test cube of edge length l and volume $V_T = l^3$ enclosing a system of randomly oriented surfaces throughout the cube [12]. The surfaces may be planar or curved, continuous or interrupted, isolated or connected, as shown in Figure 3. A set of N vertical test lines of total length $L_T = Nl$ is passed randomly through the cube, cutting horizontal planes through the cube with density N/l^3.
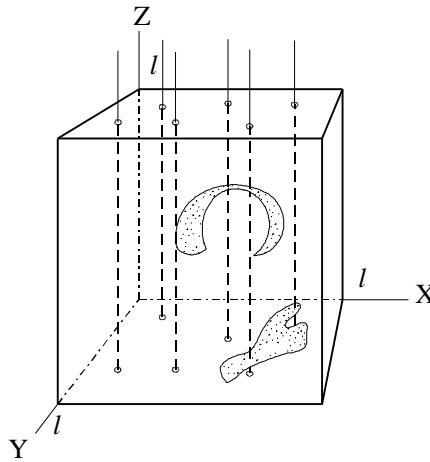

Figure 3 The cube containing random surfaces cut by random vertical test lines

The total surface, S, is divided into n elementary units of surface area dS so that $S = ndS$. The normals to each elementary area form angle q_i to the vertical test lines, and the areas of the projections of the elementary areas on a horizontal plane, equal $dS \cos q_i$. Thus the fraction of test lines intersecting the elementary areas is $dS \cos q_i / l^2$.

If P_i is the number of intersections associated with each elementary area, then the expected value of the total number of intersections with the entire surface is:

$$E(P) = \sum^n P_i = N \sum^n \frac{dS \cos q_i}{l^2} = \frac{NdS}{l^2} \sum^n \cos q_i \qquad (2)$$

Since the elementary units of surface are oriented randomly, every value of q_i has equal likelihood and $\left(\dfrac{1}{n}\right)\sum^n \cos q_i$ equals the average value, $\overline{\cos q}$. Making appropriate substitutions in Equation 2 yields:

$$E(P) = \left(\frac{N}{l^2}\right)(dSn)\overline{\cos q} \qquad (3)$$

Since $ndS = S$, and $\dfrac{N}{l^2} = \dfrac{Nl}{l^3} = \dfrac{L_T}{V_T}$, where L_T is the total length of test arrays, Equation 3 can be rewritten as:

$$E(P) = \left(\frac{L_T}{V_T}\right)S\overline{\cos q} \qquad (4)$$

where $E(P)$ is the expected value of the total number of intersections of the test lines with the system of surfaces.

The evaluation of $\overline{\cos q}$ can be visualized by means of the hemisphere with a radius of r, as depicted in Figure 4 [12]. The probability that normals lie between q and $q + dq$ is expressed by

$$P(q)dq = \frac{\text{area of zone}}{\text{area of hemisphere}} = \frac{2pr^2 \sin q dq}{2pr^2} = \sin q dq$$

and average value of $\cos q$ is

$$\overline{\cos q} = \int_0^{p/2} P(q)\cos q dq = \int_0^{p/2} \sin q \cos q dq = \frac{\sin^2 q}{2}\Big|_0^{p/2} = \frac{1}{2}$$
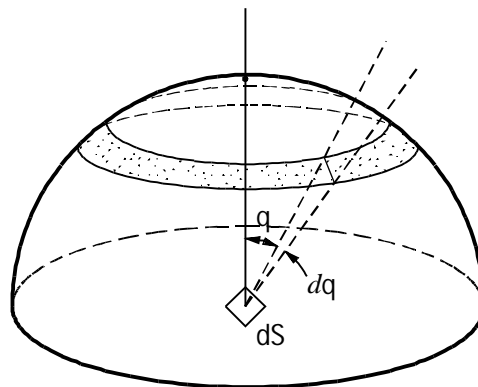

Figure 4 Geometry involved in the determination of the probability that random normals lie between q and $q + dq$

Rearrangement of Equation 4 gives

$$E(P) = \frac{L_T}{V_T}\frac{S}{2} \quad \text{or} \quad \frac{S}{V_T} = \frac{2E(P)}{L_T}$$

which yields Equation 1,

$$S_V = 2P_L \quad mm^2 / mm^3$$

- **Length of Line Per Unit Area,** L_A, relates the length of lineal elements in a plane to their intersection with a test line:

$$L_A = \left(\frac{p}{2}\right)P_L \quad mm/mm^2 \tag{5}$$

The quantity L_A is a basic microstructural parameter that is useful either as it is or when manipulated into other forms. To derive Equation 5, given a randomly oriented system of lines in a plane, let us consider a square test area A_T of edge length l as shown in Figure 5. A set of N vertical test lines of total length $L_T = Nl$ is passed randomly through the test area, cutting horizontal lines through the square with density N/l. The system of lines is divided into n straight elementary segments of length dL and the total line length in the system is $L = ndL$. The elementary segments form angle q_i to the vertical test lines, and the length of projections of the elementary segments on a horizontal line, are $dL\sin q_i$. Thus the fraction of test lines intersecting the elementary segments is $dL\sin q_i / l$. (Note that nominator L is related to 2-D structural features, e.g. crack length. In P_L, denominator L deals with length of line array).
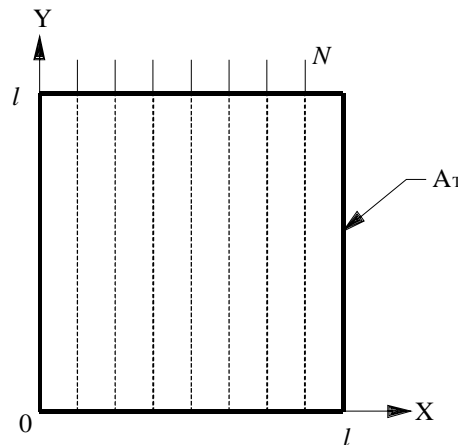

Figure 5 Model of deriving the relationship $L_A = \left(\frac{p}{2}\right)P_L$

If P_i is the number of intersections of each elementary segment by the test lines, then the expected value of the total number of intersections with the entire system of lines is

$$E(P) = \sum^{n} P_i = N \sum^{n} \frac{dL \sin q_i}{l} = \frac{NdL}{l} \sum^{n} \sin q_i \qquad (6)$$

Since the elementary systems are oriented randomly, each value of the angle q_i has equal likelihood of existence and $\left(\frac{1}{n}\right) \sum^{n} \sin q_i$ equals the average value $\overline{\sin q}$. Making appropriate substitutions in Equation 6 yields:

$$E(P) = \frac{NdLn}{l} \overline{\sin q} \qquad (7)$$

Since $ndL = L$ and $\dfrac{N}{l} = \dfrac{Nl}{l^2} = \dfrac{L_T}{A_T}$, Equation 7 can be rewritten as:

$$E(P) = \frac{L_T}{A_T} L \overline{\sin q} \qquad (8)$$

The evaluation of $\overline{\sin q}$ can be visualized by means of the circle depicted in Figure 6.
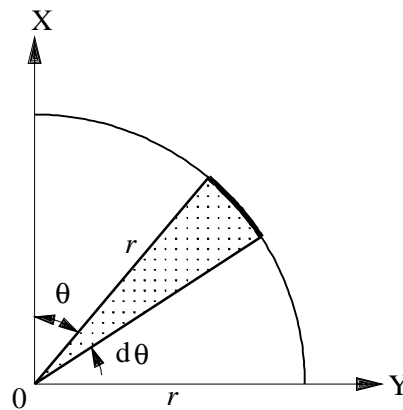

Figure 6 Geometry involved in the determination of the probability that elementary segments lie between q and $q + dq$

The probability that the elementary segments are oriented between q and $q + dq$ is equal to the fraction of the perimeter of a circle that is occupied by this orientation range. From the symmetry involved, only one quadrant of the circle needs to be considered, giving for the probability

$$P(q)dq = \frac{\text{fraction of perimeter}}{\text{perimeter of circle}} = \frac{rdq}{pr/2} = \frac{2}{p} dq$$

Thus the average value of $sinq$ is

$$\overline{\sin q} = \int_0^{p/2} P(q)\sin q\, dq = \frac{2}{p}\int_0^{p/2}\sin q\, dq = \frac{2}{p}$$

Rearrangement of Equation 8 gives

$$\frac{L}{A_T} = \left(\frac{p}{2}\right)\frac{E(P)}{L_T}\quad \text{mm/mm}^2$$

or, in our notation,

$$L_A = \left(\frac{p}{2}\right)P_L \quad \text{mm/mm}^2 \tag{9}$$

DEGREE OF ORIENTATION

Underwood [12] states that in real structures, the lines in a microsection of a given specimen are usually either isometric or partially oriented. Only in rare cases do we find completely oriented or completely random systems of lines. In a partially oriented system of lines in a plane, part of the total length of lines is oriented in a definite direction (or directions). The remaining segments may essentially have a random orientation. This is an assumption to simplify the sampling strategy. This assumption was proposed for the first time by Stroeven [16] for line elements and by Saltikov [17] for surface elements.

The lines of a partially oriented system of lines in a plane can be divided into elementary straight segments that are very small and of equal length. Some or all of the segments will lie parallel to one or more definite directions (the orientation axes). The remaining segments are assumed to be oriented randomly, or isometrically. From this point of view, a partially oriented system of lines may be regarded as consisting of two superimposed systems of lines: an oriented portion and a random portion.

In the random case, the length of linear elements in a plane is proportional to the number of intersections made with a test line. Using a test array of straight parallel lines, the number of intersections with an oriented system of lines such as a crack system in concrete will vary with the direction of the test array. The dependence of the number of intersections per unit length with the angle of the test array can be used to characterize the degree and type of orientation of a system of lines in a plane.

If a test array system of equally spaced, straight parallel lines is superimposed on a sample area, i.e., an image of the crack network in concrete, similar to Figure 3, the number of intersections per unit length of the test line P_L can be determined. Since the value of P_L is a function of the direction of the line system, the specific number of intersections is indicated as $P_L(q)$. The *rule of total projections* [16] states that this value of $P_L(q)$ equals the value of the total projected length $L_{A_{\text{Proj.}}}$ of the lineal features upon a line perpendicular to the test array, or

$$P_L(q) = L_{A_{\text{Pr}oj.}} \tag{10}$$

This type of sampling procedure is called the *method of directed secants on a plane* [17].

In the case of an isometric (randomly oriented) system, the value of $P_L(q)$ is dependent on q and both sides of equation 10 can be averaged with respect to orientation. The result is an important relationship connecting the length of lineal features in a sampling area, L_A, to the specific surface area or to the number of intersections per unit length of the test line, and averaged with respect to the orientation (note that from Equation 1, $S_V = 2P_L$). Therefore,

$$\frac{p}{2} P_L = L_A = \frac{p}{4} S_V \qquad (11)$$

Applying the method of random secants on a plane to an image of a crack pattern, Equation 11 presents simple algebraic relationships to calculate the total crack length per unit area or the specific surface area (of the cracks) per unit volume. The dependence of the number of intersections per unit length with the angle of the test array can be used to characterize the degree and types of orientation of a system of lines in a plane. Saltikov [18] proposes a polar plot of P_L with respect to the orientation axis (axes), and calls the resulting curve the *rose of the number of intersections*, or simply the *rose*.

The rose for an oriented system of lines can readily be obtained experimentally by applying a test array to the system of lines at equal angular increments with respect to the orientation axis, and determine P_L separately at each angle. A polar diagram can be made by plotting the radius vectors, P_L, versus q. The rose diagram is created by connecting the ends of the radius vectors by lines or a smooth curve. In the case of isometry, the rose will be a circle with its center at the origin of the polar figure. If a preference direction should occur in a crack pattern, the shape of the rose will change.

The stress-induced microcrack system in concrete, a composite material, is considered to be a partially oriented as opposed to a completely oriented (idealized) system.

APPLICATION OF STEREOLOGY TO CONCRETE FRACTURE

Stroeven [15, 19, 20, 21, 22, 23], Ringot [24], and Massat et al. [25] successfully applied the concept of stereology to study micromechanical aspects of concrete. With the advent of modern image analysis systems, it is now possible to perform stereological analysis on a great number of images accurately and expeditiously, whereas in the past this was not achievable by means of manual methods.

The concept of stereology, which deals with the interpretation of three-dimensional structures by means of their two-dimensional sections, was applied to analyze the backscatter electron images, obtained from SEM using an image analyzer (*Kontron Electronik GmbH Image Analysis Division, IBAS "Interaktives Bilt-Analysen System" (Interactive Image Analysis System)*). Computer programs were developed to analyze the images based on the concept of stereology. The area of the image that image analyzer analyzes is a square with the dimensions 512×512 pixels, each pixel corresponding to 3.2890 microns at ×60 magnification, which in this case is the magnification used to obtain the BSE images.

The binary image, such as the one in Figure 3, is then intersected by an array of straight parallel lines at 15° angular increments, in this case at angles of 0°, 15°, 30°, 45°, 60°, 75°, 90°, 105°, 120°, 135°, 150°, and 165°. Figure 7 depicts the array of straight parallel lines at 0° (or 180°), 15°, and 165°. The number of crack intercepts at a given angle is measured according to the number of intersections on line array at that angle with the features in the binary image, which in this case represents the crack network. The number of intersections is determined separately at each angle q. Then the number of intersections is plotted versus q, creating the rose of the number of intersections diagram. The rose diagram characterizes the degree of orientation of the cracks, and makes it easier to interpret the data.
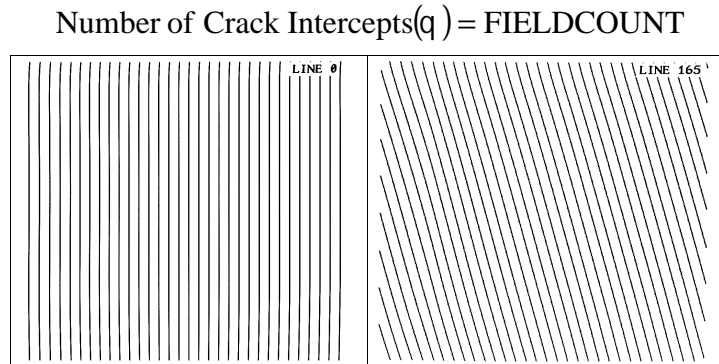
$$\text{Number of Crack Intercepts}(q) = \text{FIELDCOUNT}$$

Figure 7 Array of straight parallel lines

The program also calculates the total area of the features in the binary image. Since the area of each image is known, the percent of the area that is cracked (or, the crack density) can be determined. Figure 8 is a flow chart summarizing the above discussion.
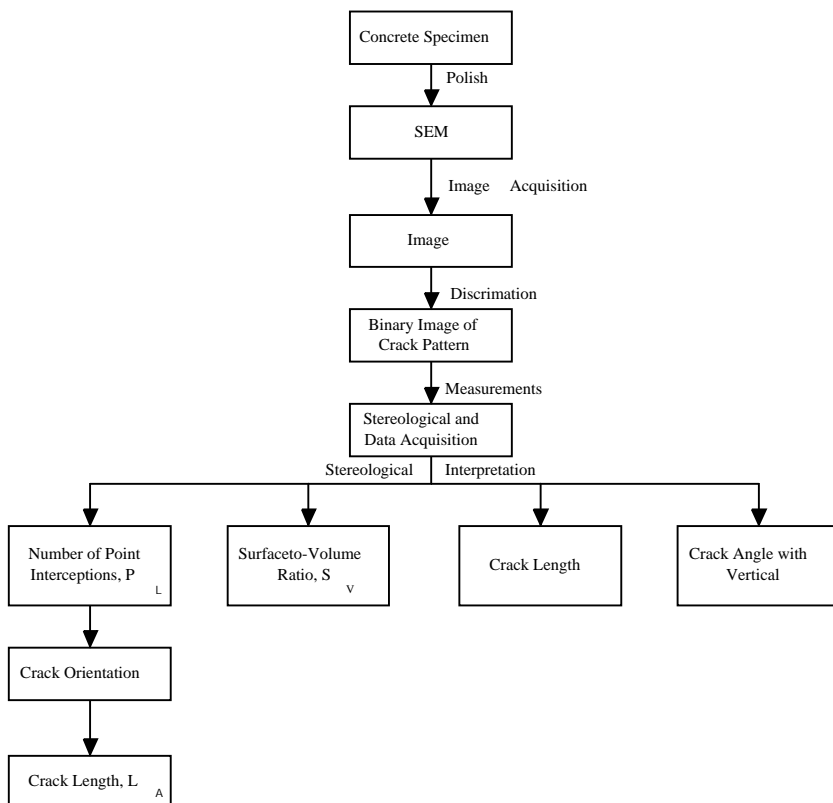

Figure 8 Flow chart for stereological steps

RESULTS

Table 2 summarizes the results of stereological analysis. As described earlier, after a binary image of the crack network is developed, that binary image is then intersected by an array of straight parallel lines at angles of 0°, 15°, 30°, 45°, 60°, 75°, 90°, 105°, 120°, 135°, 150°, and 165°. The number of crack intercepts at a given angle is measured according to the number of intersections on line array at that angle with the crack network in the binary image.

Table 2 The number of crack intercepts with the array of straight parallel lines, $P_L(q)$

Specimen	Angle of Array of Straight Parallel Lines											
Loading	0°	15°	30°	45°	60°	75°	90°	105°	120°	135°	150°	165°
No Load	31	31	29	27	29	31	30	30	28	25	28	32
Uniaxial	47	48	44	39	41	42	41	42	39	36	42	47
Confined	25	24	23	20	22	23	22	23	21	20	22	25

Table 3 shows the total area of the cracks in the binary image. Since the area of each image is known (512×512 pixel square on a SEM image), the percent of the area that is cracked (i.e., crack density) can be determined. Another value in the table below is the surface-to-volume ratio, S_V, determined from the basic equation for obtaining the area of surfaces in a volume, $S_V = 2P_L$ (only for random crack systems).

Table 3 Stereological Data

Loading	Crack Area	% Crack Area	S_V
No Load	8223	1.00	1.1E-3
Uniaxial	11843	1.53	1.6E-3
Confined	6485	0.74	8.3E-4

The stereological measurement of the surface-to-volume ratio, S_V (S/V), was determined from the basic equation for obtaining the total crack surface area per unit of volume. Plot of S_V for different loading conditions are presented in Figure 9. Crack surface area, S_V, decreases as the confining stresses is introduced.
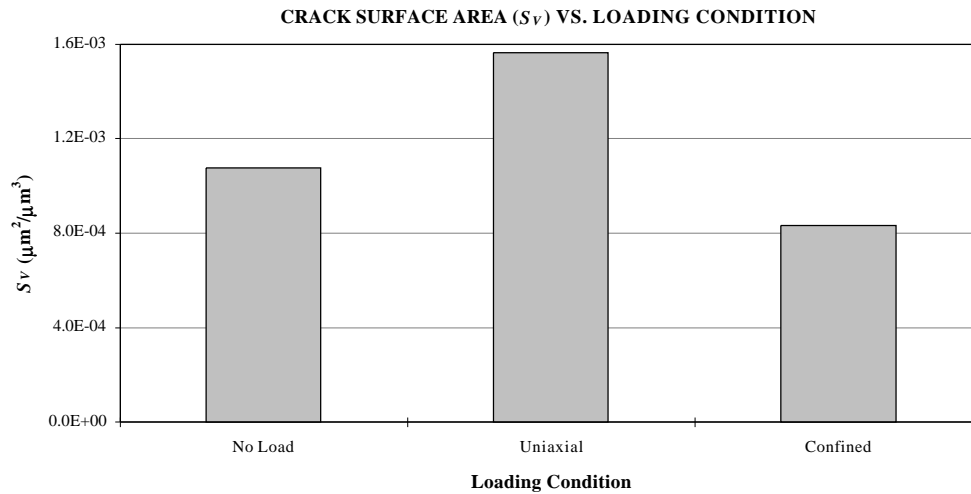
CRACK SURFACE AREA (S_V) VS. LOADING CONDITION

Figure 9 Crack surface area (S_V) as a function of loading condition

Based on stereological analysis, L_A, the length of line per unit area also decreases with presence of confining stresses. The average length distribution of the microcracks strongly depends on the confining stress. Because the microcracks are produced by local tensile stresses, the driving forces from the local tensile stresses decrease as the microcrack length increases. On the other hand, the negative driving forces applied by the confining stress increase as the microcrack length increases. The combined effect of these two arguments is a great reduction in microcrack length under high confining stress.

In the specimen subjected to uniaxial compression, most of the microcracks propagated to a certain length and stopped. When confining stress was introduced, the average length of the microcracks decreased, as indicated in Figure 10. It shows clearly that the average length distribution of microcracks is strongly dependent on the confining stress.
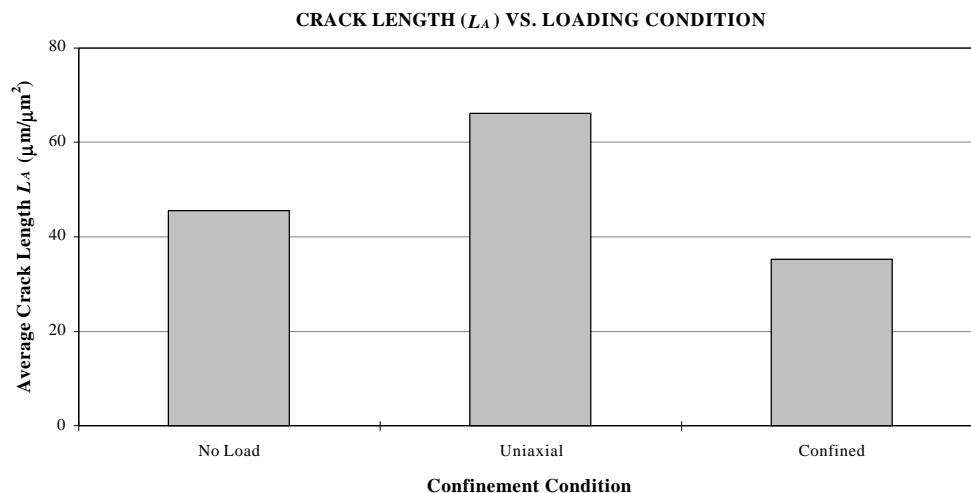
CRACK LENGTH (L_A) VS. LOADING CONDITION

Figure 10 Stereological measurement of crack length as a function of loading condition

One way to determine the anisometry of the crack network, $P_L(\theta)$, is to plot it in a polar figure according to the specific orientation of the cracks. The plot of number of intersections versus orientation (in 12 equal angle steps) covers only the range of 0° to 165° (cracks at 0° and 180° have equal lengths) since the range from 180° to 360° is redundant. This information is shown in different format than most distribution plots because the *compass rose* pattern makes it easier to interpret the data. A so-called *rose of the number of intersections* is constructed in this way. Figure 11 shows the rose of the number of intersections for the reference (no load), uniaxially, and triaxially loaded concrete samples. From Figure 11 it is evident that cracks are not randomly oriented and there is a definite orientation in the crack pattern. Many cracks lie within 15 degrees of the direction of the maximum compression (between 0° and 15° and 165° and 180°) than in other directions.
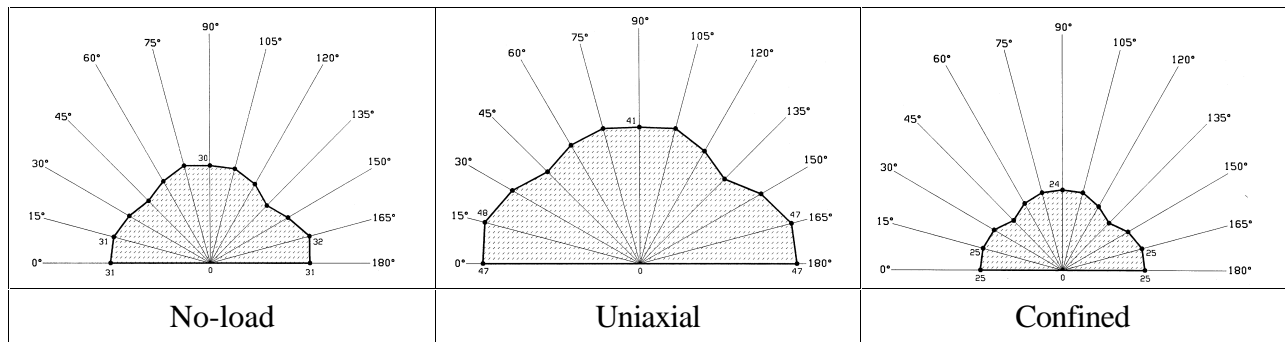
No-load	Uniaxial	Confined

Figure 11 Rose of the number of intersections diagrams for reference and uniaxially-loaded concrete specimens

Crack density can be measured in terms of percent cracked area. Figure 12 is the plot of percent cracked area as a function of loading condition. Again, percent cracked areas decrease as the confinement is introduced. The reference specimen (no-load sample) has a relatively high crack density due to the fact that concrete is heavily cracked even before applying any load (Hsu et al. 1963). Hence, the effective crack density increase for the specimen subjected to applied loads is the difference between the final crack density and the crack density of the no-load specimen.
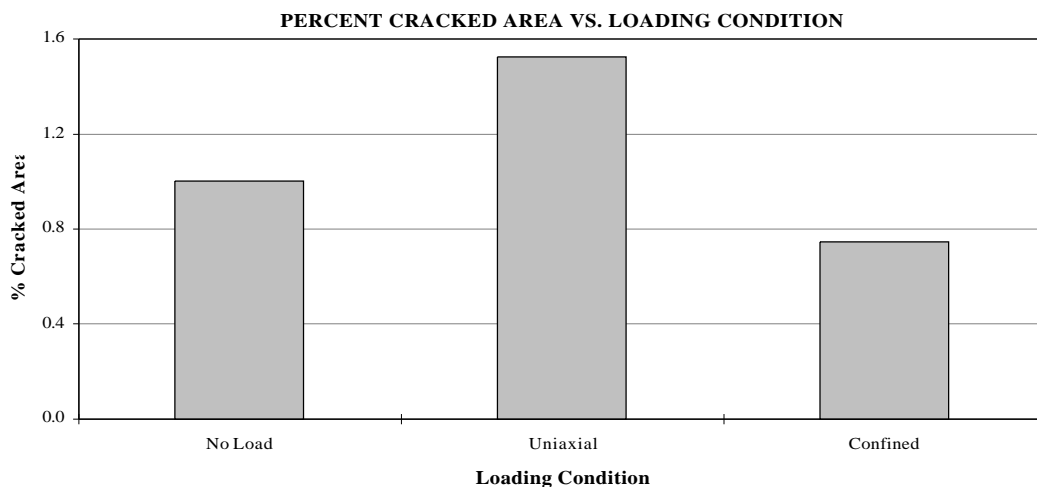
Figure 12 Percent cracked area as a function of loading condition

CONCLUDING REMARKS

The stereological approach to the study of mechanical behavior of concrete was examined here. By analysis of BSE images and the application of stereology, various measures of the crack surface area per unit volume, crack length, crack orientation and crack density were obtained. The measured surface area of cracks increased when the specimens were loaded uniaxially. Confinement decreased the crack density. Crack orientation measurements indicated slight orientation, however, the cracks were relatively isotropic at a microscopic level, which is due the domination of transition zone microcracks which are randomly oriented.

Stereology is a powerful tool to study mechanical behavior of engineering materials and its application in the field of concrete technology should be further explored.

REFERENCES

1 Le Chatelier, H. (1882). "Experimental Researches on the Constitution of Hydraulic Mortars," translated by J. L. Mack, McGraw, New York, 1905. Also: Compt. rend., 94 (1882) 13; and *Journal of Chemical Ind.*, 1 (1882) 151.

2 Tavasci, B. (1942). "Structure of Hydrated Portland Cement," *Zement*, Vol. 30, No.4, 43-48 & 55-58.

3 Eitel, W. (1941). "Recent Results of Cement Research," *Angewandte Chemie*, Vol. 54, No. 15/16, 185–192.

4 Eitel, W. (1942). "Electron Microscopic Cement Research," *Zement*, 31, 489–495.

5 Radczewski, O. E.; Müller, H. O.; and Eitel, W. (1939). "Ultra-Microscopic investigation of the Hydration of Free Lime," *Zement*, Vol. 28, No. 49, 693–697.

6 Grudemo, A. (1960). "The Microstructure of Hydrated cement Paste," *Proceedings, Fourth International Symposium on the Chemistry of Cement*, 2, 615–658, Washington, D.C.

7 Diamond, S., and Mindess, S. (1980) "A Preliminary SEM Study of Crack Propagation in Mortar", *Cement and Concrete Research*, Vol. 10, No. 4, 509–519.

8 Nemati, K.M. (1994). "Generation and Interaction of Compressive Stress-Induced Microcracks in Concrete," *Ph.D. Thesis*, Department of Civil Engineering, University of California at Berkeley.

9 K.M. Nemati, P.J.M. Monteiro, and N.G.W. Cook (1998). "A New Method for Studying Stress-Induced Microcracks in Concrete," American Society of Civil Engineers, Journal of Materials in Civil Engineering, Vol. 10, No. 3, 128-134.

10 K.M. Nemati, P.J.M. Monteiro, and K.L. Scrivener (1998). "Compressive Stress-Induced Fracture Generation And Interaction In Concrete," American Concrete Institute Materials Journal, Vol. 95, No. 5, 617-631.

11 K.M. Nemati (1997). "Fracture Analysis of Concrete Using Scanning Electron Microscopy," Scanning, The Journal of Scanning Microscopies, Vol. 19, No. 6, 426-430.

12 Underwood, E. E. (1968). "Quantitative Stereology," Addison-Wesley Publishing Company, New Jersey.

13 Russ, John C. (1986). "Practical Stereology," Plenum Press, New York.

14 Saltikov, S. A. (1945). "Stereometric Metallography," second edition, Metallurgizdat, Moscow.

15 Smith, C. S.; and Guttman, L. (1953). "Measurement of Internal Boundaries in Three Dimensional Structures by Random Sectioning," *Trans. AIME* ,197.

16 Stroeven, P. (1973). "Some Aspects of Micromechanics of Concrete," PhD Thesis, Stevin Laboratory, Technological University of Delft.

17 Saltikov, S. A. (1967). "A Stereological Method for Measuring the Specific Surface Area of Metallic Powders, Stereology, edited by H. Elias, *Proc. Second International Congress for Stereology*, Chicago; Springer Verlag, New York.

18 Saltikov, S. A. (1945). "Stereometric Metallography," second edition, Metallurgizdat, Moscow.

19 Stroeven, P. (1976). "Application of various stereological methods to the study of the grain and the crack structure of concrete," *Journal of Microscopy*, 107(3), 313–321.

20 Stroeven, P. (1976). "Morphometry of plain and fibre reinforced concrete by means of image analysis techniques," *Proceedings of the second International conference on Mechanical Behavior of Materials*, Boston, Massachusetts, 1675–1679.

21 Stroeven, P. (1979). "Geometric probability approach to the examination of microcracking in plain concrete," *Journal of Materials Science*, 14, 1141–1151.

22 Stroeven, P. (1991). "Fractals and Fractography in Concrete Technology," *International Symposium on Brittle Matrix Composits*, 3rd, Warsaw, Poland, 1–10.

23 Stroeven, P. (1992). "Some mechanical effects of interface debonding in plain concrete, Interfaces in Cementitious Composits," *Proceedings of the RILEM International Conference*, Edited by J.C. Maso, Toulouse, France, 187–196.

24 Ringot, E (1988). "Automatic quantification of microcracks network by stereological method of total projections in mortars and concretes," *Cement and Concrete Research*, 18, 35–43.

25 Massat, M.; Ollivier, J.P.; and Ringot E. (1988). "Microscopic Analysis of Microcracking Damage in Concrete and Durability," *Laboratoire Materiaux et Durabilite des Constructions (INSA-UPS)*, Toulouse, France.